Pergamon

Geochimica et Cosmochimica Acta, Vol. 65, No. 1, pp. 63–74, 2001

0016-7037/01 $20.00 + .00

PII S0016-7037(00)00525-1

Nanoforms: A new type of protein-associated mineralization

HOJATOLLAH VALI,[1,2,3] MARC D. MCKEE,[2,4] NEVA ÇIFTÇIOGLU,[5] S. KELLY SEARS,[1,2,3] FIONA L. PLOWS,[6] ERIC CHEVET,[2] PEGAH GHIABI,[2] MARC PLAVSIC,[7] E. OLAVI KAJANDER,[5] and RICHARD N. ZARE[6]

[1]Electron Microscopy Centre, McGill University, 3640 University Street, Montréal, QC H3A 2B2, Canada
[2]Department of Anatomy and Cell Biology, McGill University, Montréal, QC H3A 2B2, Canada
[3]Department of Earth and Planetary Sciences, McGill University, Montréal, QC H3A 2A7, Canada
[4]Faculty of Dentistry, McGill University, Montréal, QC H3A 2B2, Canada
[5]Department of Biochemistry, University of Kuopio, FIN-70211, Kuopio, Finland
[6]Department of Chemistry, Stanford University, Stanford, CA 94305-5080, USA
[7]Life Technologies, Grand Island, NY 14072, USA

(*Received February* 8, 2000; *accepted in revised form July* 20, 2000)

Abstract—Controversy surrounds the interpretation of various nano-phenomena as being living organisms. Incubation of fetal bovine serum under standard cell culture conditions results in the formation of free entities in solution, here referred to as nanoforms. These nanoforms, when examined by transmission electron microscopy, have a distinct ovoid morphology ranging in size from tens to hundreds of nanometers. They are composed of hydroxyapatite and proteins and constitute a novel form of protein-associated mineralization. No detectable cell structure resembling bacteria is apparent. However, immunodetection of the proteins associated with the nanoforms, by two specific monoclonal antibodies, suggests a possible biogenic origin. The significance of nanoforms for the recognition of biological activity in ancient geological systems is discussed. The mode of mineralization in nanoforms is also compared to matrix-mediated calcification in vertebrates. *Copyright © 2001 Elsevier Science Ltd*

1. INTRODUCTION

Inspired by questions about the nature of nanoscale mineralized forms and textures observed in Martian meteorite ALH84001 (McKay et al., 1996), we have undertaken a detailed examination of mineralization events that result in the formation of nanoforms. Nanoforms, described previously in various geological and biologic systems as nan(n)obacteria (Folk, 1993; Pedone and Folk, 1996; Sillitoe et al., 1996; Folk and Lynch, 1997; Kajander and Çiftçioglu, 1998), nanofossils (McKay et al., 1996; Bradley et al., 1997; Vali et al., 1999), nanobes (Uwins, 1998), fossil nan(n)obacteria, and nano-organisms, is the descriptor that we have adopted to encompass all nano-sized mineralized forms, whether these structures are animate or inanimate objects.

Two areas of study regarding the mineralization phenomenon relevant to nanoforms are apparent in the literature. Both describe mineral formation in what are thought to be biologic systems. Firstly, minerals precipitated within geological systems and having morphologic features distinct from inorganic precipitants have been suggested to be caused by, or intimately associated with, nan(n)obacteria. McKay et al. (1996) proposed, therefore, that the similarity in morphology between the nanometer ovoid and elongate features observed in the fractured surfaces of the Martian meteorite ALH84001 and the nan(n)obacteria of Folk (1993) was evidence for the existence of microbial life on Mars. Without structural or molecular data, however, many researchers have argued that a biologic origin for these nan(n)obacteria is speculative.

Secondly, in another investigation involving nanoforms, Kajander and Çiftçioglu (1998) reported that the *Nanobacterium sanguineum* isolated from human and cow sera produced a protective, mineralized outer shell-like structure that protected this organism from otherwise lethal, microbiological sterilization. Results of 16S rRNA gene sequencing (EMBL X98418 and X98419) indicate that it belongs to the α 2 subgroup of proteobacteria—a category that includes *Brucella* and *Bartonella* (Kajander and Çiftçioglu, 1998). The size of these nanoforms is in the range of 50 to 200 nm in diameter. The mineralized shells are on the order of tens of micrometers. A major concern in any discussion of the validity of characterizing phenomena as nan(n)obacteria is the lower limits of size for free-living microorganisms (Folk, 1997; Maniloff, 1997; Nealson, 1997; Psenner and Loferer, 1997). In a workshop convened at the National Academy of Sciences in 1998 to discuss the limits in size of very small microorganisms, it was generally agreed that the minimal size for a microorganism was likely in the range of 200 to 300 nm in diameter for a cell operating by known molecular rules (de Duve and Osborn, 1999; Nealson, 1999). It was also suggested, however, that primitive microorganisms based on a single-polymer system could be as small as 50 nm in diameter (Orgel and Ost, 1999).

Irrespective of the debate over the size limits of life, a surprisingly unique property of the nan(n)obacteria described above is a reported ability to induce biogenic formation of hydroxyapatite (HAP). Although the nature and formation of the HAP phase is not well understood, in this case it has been proposed to be responsible for the formation of kidney stones (Çiftçioglu et al., 1999) and various other pathogenic calcifications (Kajander and Çiftçioglu, 1998; Hjelle et al., 2000).

In the present study, we report on the existence, formation, structure, and composition of a unique protein/HAP-containing nanoform derived from cultured serum and demonstrate the associations of the HAP phase with specific protein compo-

*Author to whom correspondence should be addressed (vali@pebbles.eps.mcgill.ca).

nents. Here the immunolocalization of the proteins is shown by the reaction of the two specific monoclonal antibodies produced in response to mouse injected with the mineralized nanoforms observed by Kajander and Çiftçioglu (1998).

Elucidating the mechanisms of mineralization in this system will have direct implications for understanding the processes of fossilization and biomineralization in terrestrial and extraterrestrial systems. For example, fossils with well-preserved morphologic features that resemble the remains of modern microorganisms are used to trace evolutionary pathways and events in biotic history. Fossilization of microorganisms cannot occur, however, if suitable conditions for their preservation are not attained. In the absence of well-preserved genetic material required for the polymerase chain reaction method in molecular phylogenetic studies (Pace, 1997), protein-mineral interactions (biomineralization) may offer an alternative approach for the recognition of biogenic activity, both in a geological and biologic context.

Formation mechanisms involved in micro- and nano-scale mineralization that are not totally inorganic are of two types. Firstly, in the area of bacterial biomineralization, two modes of biomineralization have been distinguished: bacteria-induced and bacteria-controlled biomineralization (Lowenstam, 1981, 1986). In bacteria-induced processes, changes to the environment as a result of the metabolic activity of a bacterial cell can lead to the nucleation and growth of extracellular (bio)minerals; the mineral phases are not directly associated with cellular structures. In bacteria-controlled systems, biominerals crystallize intracellularly or on the cell walls. Biomineralization in magnetotactic bacteria (Blakemore, 1975; Vali and Kirschvink, 1990) and in cyanobacteria, *Scytonema Julianum*, (Lowenstam, 1986) are two important examples of intracellular mineralization. The kinetics of reaction and the thermodynamic processes responsible for biomineralization, however, are poorly understood. Recent studies have shown that the functional groups of proteins and lipids present in the cell walls of bacteria play a significant role in the mobilization and transport of ions involved in both extracellular and intracellular mineralization (Fein et al., 1997; Warren and Ferris, 1998; Fein and Delea, 1999). This has implications for the second type of mechanism of mineral formation, the area of biomimetics. In this case, mineralization at the inorganic–organic interface is studied in the absence of cell activity (e.g., Mann et al., 1991, 1993; Oliver et al., 1995; Hunter et al., 1996; Mann and Ozin, 1996; Walters et al., 1997; Mann and Weiner, 1999).

2. ANALYTICAL TECHNIQUES

2.1. Growth of Nanoforms

The early stage of growth of nanoforms was studied on samples obtained from three independent laboratories at McGill University, Life Technologies, and University of Kuopio. Nanoforms were collected from pure fetal bovine serum (FBS) and from a mixture of FBS and Dulbecco's modified eagle growth medium (DMEM) (1:10 ratio; typically used for eukaryotic cell culture studies) incubated for 1 month under the same cell culture conditions (5% CO_2 at 37°C and 100% humidity). The presence of mineralized nanoforms was confirmed with an inverted optical light microscope operating in the phase contrast mode at magnifications of ×25 and ×40.

The formation and growth of nanoforms were studied in 96-well, flat-bottom cell culture plates against a turbidity equivalent to that of 0.5 McFarland standard (OD650: 0.020) in microtitration wells. The tests were made in triplicate, and each 96-well plate contained uninoculated medium as a sterility control. The plates were incubated at 37°C in an atmosphere of 5% CO_2−95% air for 14 d. Growth was monitored at intervals of 0, 4, 8, 12, and 14 d. To eliminate condensation, the plate lid was warmed with a metal plate before the absorbance measurement. The chemical composition of the FBS before and after incubation was determined by calorimetry, atomic adsorption spectroscopy, and enzymatic assay. Changes in [Ca] and [P] in the supernatant remaining after centrifugation of the nanoforms from growth medium were measured by using atomic adsorption spectroscopy and calorimetry, respectively.

2.2. Electron Microscopy

Pellets of nanoforms were obtained from the 1-month incubated specimens by centrifugation techniques (15,000 *g* for 5 min) and investigated by transmission electron microscopy (TEM). The pellets were washed several times with 0.1 mol/L sodium cacodylate buffer (pH = 7) and then deionized water to remove excess serum. Specimens were prepared by transferring 5 μL of re-dispersed pellet onto formvar- and carbon-coated Cu grids. To study the internal structure of the nanoforms, 50 μL of a concentrated suspension of nanoforms was dehydrated in alcohol, embedded in epoxy resin (Epon 812, Marivac Inc., Canada) and sectioned by using an ultramicrotome (Reichert-Jung Ultracut E, Vienna, Austria). High-resolution transmission electron microscopy (HRTEM) and selected-area electron diffraction (SAED) were used to characterize the mineral phases in the sample by using a JEOL 2000FX TEM (Tokyo, Japan) operating at 200 kV in bright-field mode and at Scherzer defocus conditions. The chemical composition was qualitatively determined by energy dispersive spectroscopy (EDS). The X-ray spectra were acquired with an electron beam size of 200 nm at 80 kV for 100 s. Additionally, cryo-fixation (Bachmann, 1987) and freeze-etch (Moor and Muehlethaler, 1963) techniques were applied to investigate the morphology of the nanoforms. These latter techniques are advantageous in that they allow the investigation of the hydrated systems in their original state. They have been successfully applied to investigate the growth characteristics of clay minerals and carbonates (Vali and Bachmann, 1988; Vali et al., 1991; Paquette et al., 1996, 1999). Moreover, the resolution of the Pt-C replicas obtained from these approaches is at the nano-scale, a resolution that is an order of magnitude greater than that obtained by conventional scanning electron microscopy (SEM). The morphology of the larger forms was imaged by using a Hitachi 4700 field emission gun SEM (FEGSEM) operating at 0.7 kV without any coating.

2.3. Ultrastructural Immunolocalization

Cryo-ultrathin sections combined with immunogold labeling were used for protein localization by using anti-nan(n)obacteria monoclonal antibodies (Nb 8/0 and Nb 5/2; Kajander and Çiftçioglu, 1998). In contrast to the embedding of biological specimens with low-viscosity resin in the preparation of ultrathin sections that results in the alteration of the functional groups of proteins, cryo-ultrathin sectioning enables the investigation of the protein in its natural configuration. In this technique, the pellet is embedded in sucrose and frozen at −196°C and sectioned at −150°C by using an ultracryomicrotome (Reichert-Jung Ultracut FC 4D). The ultrathin sections are transferred to formvar- and carbon-coated Cu grids. To localize the specific protein with known antibodies, the grids are exposed to a primary antibody that can be recognized by commercially available secondary antibody that is coupled to a particle of colloidal gold. Only the proteins binding to primary antibodies will be labeled with the gold marker. To investigate specificity of the immunolabeling in control incubations, the primary antibody was omitted from the incubation procedure.

2.4. Sample Preparation for Immunoprecipitation

Aliquots (5 mL) of the incubated FBS/DMEM mixture were centrifuged at 50,000 rpm in a sw60 rotor (Beckman, Fullerton, CA, USA) for 3 h. Pellets containing the HAP precipitate were washed three times in water and resuspended in 1 mL phosphate buffered saline containing 2 mM ethylene diamine tetracetic acid, 1 mM phenylmethylsulfonyl fluoride, Leupeptin, Aprotinin at 1 μg/mL (protease inhibitors), then

sonicated 2 × 30 s using a Vibra-Cell (Danbury, CT, USA) sonicator with the 2.5 mm probe, and the non-ionic detergent Triton X-100 was added to a 1% final concentration. For denaturing conditions, the ionic detergent sodium dodecyl sulfate (SDS) was added to the sonicated sample (1% final concentration), incubated for >20 min at 4°C, and then before immunoprecipitation this sample was diluted 15 times with phosphate buffered saline containing 1% Triton X-100.

2.4.1. Immunoprecipitation

The samples (as prepared above) were centrifuged in a microcentrifuge at 14,000 rpm for 15 min, and the supernatant was precleared for 1 h at 4°C with protein G Sepharose beads to remove nonspecific binding to protein G. After incubation, the beads were removed by centrifugation and the supernatant was incubated overnight at 4°C with the mouse monoclonal antibodies Nb 8/0 or Nb 5/2 (1:100 dilution). Protein G Sepharose beads were added for 1 h at 4°C to purify the immune complexes containing Nb 8/0 or Nb 5/2 antibodies, centrifuged, and washed 5 times with phosphate buffered saline containing 0.1% TX-100. After removal of supernatant, the immune complexes bound to the beads were resuspended in 50 μL of Laemmli sample buffer containing 0.1 mol/L Tris-HCl pH 6.8, 2% SDS, 100 mM β-mercaptoethanol, 10% glycerol and 0.1% bromophenol blue (Laemmli, 1970), and heated at 95°C for 5 min. The proteins contained in these immune complexes were resolved by using SDS–Polyacrylamide gel electrophoresis according to their molecular mass (Laemmli, 1970). The immunoprecipitated material was visualized by Coomassie blue R-250 or silver nitrate staining of the gels.

3. RESULTS

Incubation of FBS results in the formation of mineralized HAP nanoforms dispersed in solution with some additional material adhering to the incubation vessel. Incubation of the mixture of FBS/DMEM, at a ratio of 1:10, results in increased mineralization of the nanoforms relative to incubation in FBS alone. To study the mechanism of nucleation and growth of HAP and its association with the organic matrix, we focused our investigation on the suspended nanoforms collected from both the pure FBS and the 1:10 FBS/DMEM mixture. Nanoforms were not initially visible with an inverted optical light microscope at a magnification of up to ×400, but mineralized nanoforms were observed after ~7 d of incubation. Except for Brownian motion, the nanoforms showed no detectable motility. After ~30 d of incubation, a distinct cloudiness was visible within the incubation vessel. The rate of growth of nanoforms was assessed by measuring the increase in turbidity of the growth medium (Fig. 1). Examination of the growth medium by TEM revealed the presence of rough-appearing ovoid forms (hereafter referred to as nanoform type 1) consisting predominantly of a polycrystalline, plate-like HAP phase (Fig. 2a). The high contrast of these unstained forms was the result of dense mineralization. Individual crystals within the nanoforms showed a thin, plate-like morphology sometimes with a variable degree of curling at the edges of the crystal owning to dehydration and drying artifacts induced by sample preparation procedures (Fig. 2b). Selected-area electron diffraction patterns and high-resolution lattice fringe imaging of nanoform type 1 indicated a mainly two-dimensional, semioriented appearance of the crystalline phases. The overall dimensions of the lattice fringes with uniform spacing were larger than the grain size of the individual crystals, indicating some degree of hierarchical organization to crystal growth in this system (Fig. 3a,b). The *d*-spacings of the lattice fringes and selected-area electron diffraction patterns correspond to a carbonate HAP phase (Table 1). Owing to the limited amount of material available in the growth medium, we were unable to obtain an X-ray diffraction pattern of the HAP crystals present in nanoform type 1. Microanalysis of nanoform type 1 revealed the presence of Ca and P with a Ca/P ratio of 1.7–1.9, which provides additional support for the presence of carbonate HAP within nanoform type 1 (Fig. 4a,b,c). In addition to HAP, a polycrystalline structure consisting of an extremely fine crystalline phase (2–3 nm in size and lattice fringes with *d*-spacings of ∽0.3 nm) was observed in HRTEM (Fig. 3c). However, the nature of this phase could not be determined.

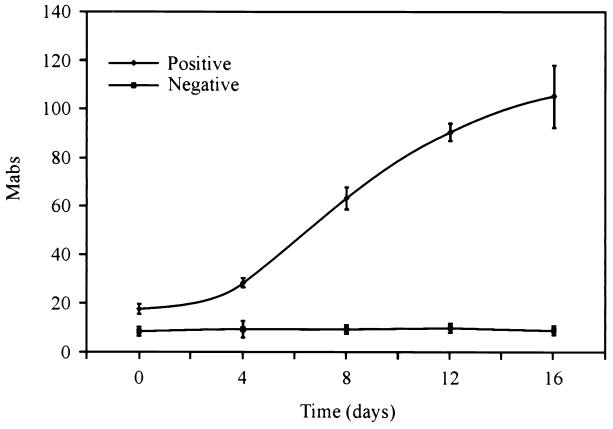

Fig. 1. The increase in the number of nanoforms with time in the 1:10 FBS/DMEM mixture. The increase in turbidity was measured in 96-well, flat-bottom cell culture plates by using 0.5 McFarland standard (OD650: 0.20) in microtitration wells.

Although nanoforms were observed to be as small as a few tens of nanometers, in a given incubation condition, the majority (∽90%) of nanoforms had the same size, which was ~200 nm. Untreated and unstained nanoform specimens appeared as a network of a high-contrast, solid mineral phase and a low-contrast organic component. After conventional staining of the specimens with uranyl acetate and lead citrate, a significant increase in contrast was observed, which suggested an association between the presence of proteins and HAP in the nanoforms (see also below). Nanoform type 1 lacked any apparent features that may be considered as being distinctly cellular in nature. TEM images of Pt–C replicas obtained from freeze-fractured pellets collected from the 1:10 FBS/DMEM mixture incubated for 1 month also showed the external surface (Fig. 5a,b) and the internal crystalline nature with a layered structure on the fractured surface of nanoform type 1 (Fig. 5c,d).

The presence and preservation of protein components in the nanoform type 1 after dissolution of the mineral phase were demonstrated by immunolabeling and immunoprecipitation. Two specific monoclonal antibodies produced in response to mouse inoculation with the SF culture (Kajander and Çiftçioglu, 1998) were used for these experiments. TEM immunolabeling was performed on conventional ultrathin cryosections resulting in poor labeling. A new preparation technique that involved adsorption of nanoforms onto formvar- and carbon-coated Cu grids was developed (Fig. 6a,b). The specificity of the association of gold particles (from secondary antibody conjugates) with the associated proteins was determined by the removal of the mineral phase after exposure of the nanoforms

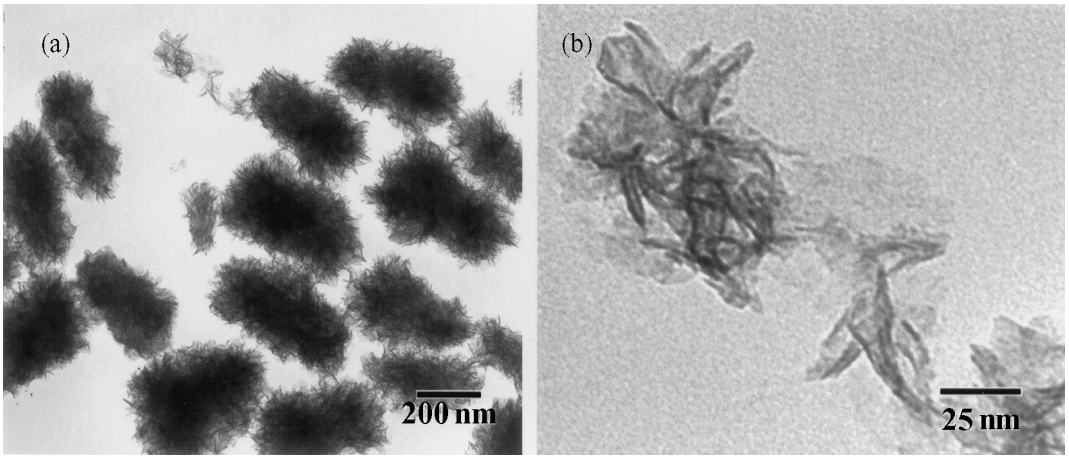

Fig. 2. TEM images of air-dried specimens of nanoform type 1, obtained from the FBS cultures adsorbed onto formvar and carbon supported Cu grids. (a) Original contrast (no staining) image shows a homogeneous size distribution of up to a maximum of ~200 nm for nanoform type 1. (b) Higher magnification of (a) (upper center) shows the aggregation of a plate-like structure in nanoform type 1. The edges of these thin layers are curled as a result of dehydration during sample preparation. The "hairy" appearance of nanoform type 1 is partly also attributed to the curling of thin layers.

to a 0.1 N HCl solution before and/or after immunogold labeling in which labeling was retained in the absence of mineral. TEM immunolabeling was also performed by using antibodies raised against other mineral-binding proteins found in bone, serum, and other tissue fluids. The antibodies used were three polyclonal antibodies against osteopontin (OPN), and two polyclonal antibodies against serum fetuin(α_2HS-glycoprotein); goat anti-rat smooth muscle cell OPN (courtesy of Dr. Cecilia Giachelli, University of Washington, Seattle, WA); rabbit anti-human milk OPN (courtesy of Dr. Donald Senger, Beth Israel Hospital, Boston, MA); rabbit anti-rat recombinant OPN (courtesy of Dr. Charles Prince, University of Alabama, Birmingham, AL); and rabbit anti-human serum fetuin and rabbit anti-mouse serum fetuin (courtesy of Dr. Willi Jahnen-Dechent, University of Mainz, Germany). None of these antibodies showed specific binding to nanoforms.

The incorporation of organic and inorganic molecules in the nanoforms was also confirmed by chemical analysis of the

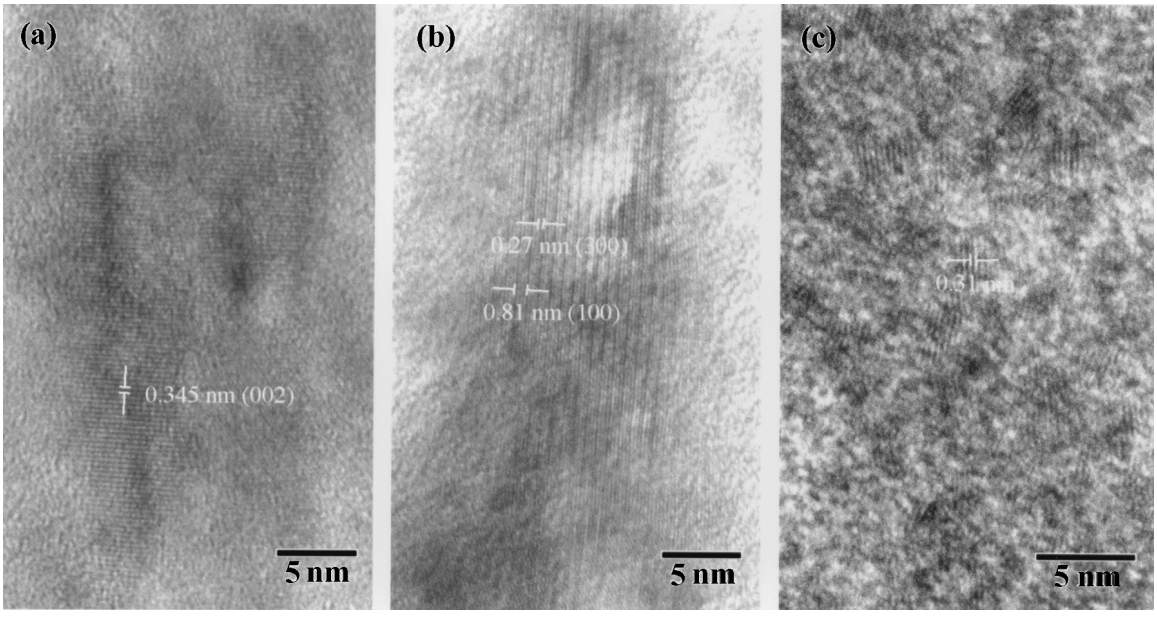

Fig. 3. HRTEM images of nanoform type 1: (a) Lattice fringes of the apatite phase. Although the same lattice fringes can be seen in many crystals, the lattice fringes of individual crystals are not always coherent with respect to each other. The one-dimensional alignment of most crystals in the **c**-direction indicates preferential growth of the crystals in the **c**-direction. (b) View of an apatite crystal in the crystallographic **a**-direction showing *d*-spacings of 0.81 nm (100) and 2.78 nm (300). This type of structure has been observed in crystals of enamel. (c) Polycrystalline structure of an unknown phase having a *d*-spacing of ~0.31 nm.

Table 1. *d*-Spacings (nm) of hydroxyapatite.

PDF[a]	HRTEM	SAED	hkl
0.817	0.810		100
0.344	0.345		002
0.308		0.305	210
0.2778		0.276	112
0.2720	0.270	0.271	300
0.2528		0.249	301
0.2000		0.200	203
0.1871		0.186	320
0.1722		0.171	004,411
0.1684		0.168	104
0.1587		0.157	501,204
0.1503		0.150	214,421

[a] Powder Diffraction File Database

growth medium (supernatant) before and after incubation. A significant decrease in [Ca] and [P_i] (inorganic phosphate) as well as some of the organic components was observed between incubated and non-incubated FBS solutions, suggesting the incorporation of certain inorganic and organic components into nanoform type 1 (Table 2). In the 1:10 FBS/DMEM mixture, [Ca] decreased from 2.1 mM to 1.15 mM and [P_i] from 0.9 mM to 0.6 mM after incubation of 4 weeks. The amount of Ca consumed in the formation of the HAP component increased faster within the first week than subsequent weeks, and achieved equilibrium after 3 weeks, when approximately 50% of the available Ca and P_i in the growth medium was consumed. This is in agreement with the TEM results of the solid phase (nanoform type 1), which showed maximum concentration of the nanoforms after 4 weeks. With the addition of fresh growth medium (FBS/DMEM mixture or DMEM), the number and size of the nanoforms increased again until a new steady-state was attained. The media was maintained at a pH = 7.3–7.5 during incubation of the samples by a constant flow of 5.0% CO_2–95% air mixture. After normalization and excluding water and organic components, the nanoforms had a mean composition of 60% Ca, 35% P, 4% Mg, and 1% minor elements.

Additional biochemical analyses of the 1:10 FBS/DMEM mixture using immunoprecipitation and immunoblotting techniques confirmed the presence of protein in the nanoforms. Immunoprecipitation by using antibody Nb 8/0 showed two specific proteins (Fig. 7, lane 2). The band labeled by an open arrow is not specific and may correspond primarily to serum albumin (data not shown). Antibody Nb 8/0 was unable to recognize denatured proteins in immunoblotting experiments, suggesting a conformation-specific idiotype. These data suggest that the immuno-gold labeling observed by electron microscopy (Fig. 6a) is associated with a protein-based motif, which may be involved in the crystallization of HAP and in the biomineralization process of HAP nanoforms. Immunoprecipitation, in both native and denaturing conditions, with antibody Nb 5/2 resulted in the visualization of a major band corresponding to a protein of approximately 35 kDa (Fig. 7, lanes 4 and 5). The true nature of the proteins against which the antibody was directly raised is as yet unknown. However, it is important to emphasize that these two proteins may be in a complex and antigenic for the antibody and that they remain in a stable configuration during the immunoprecipitation.

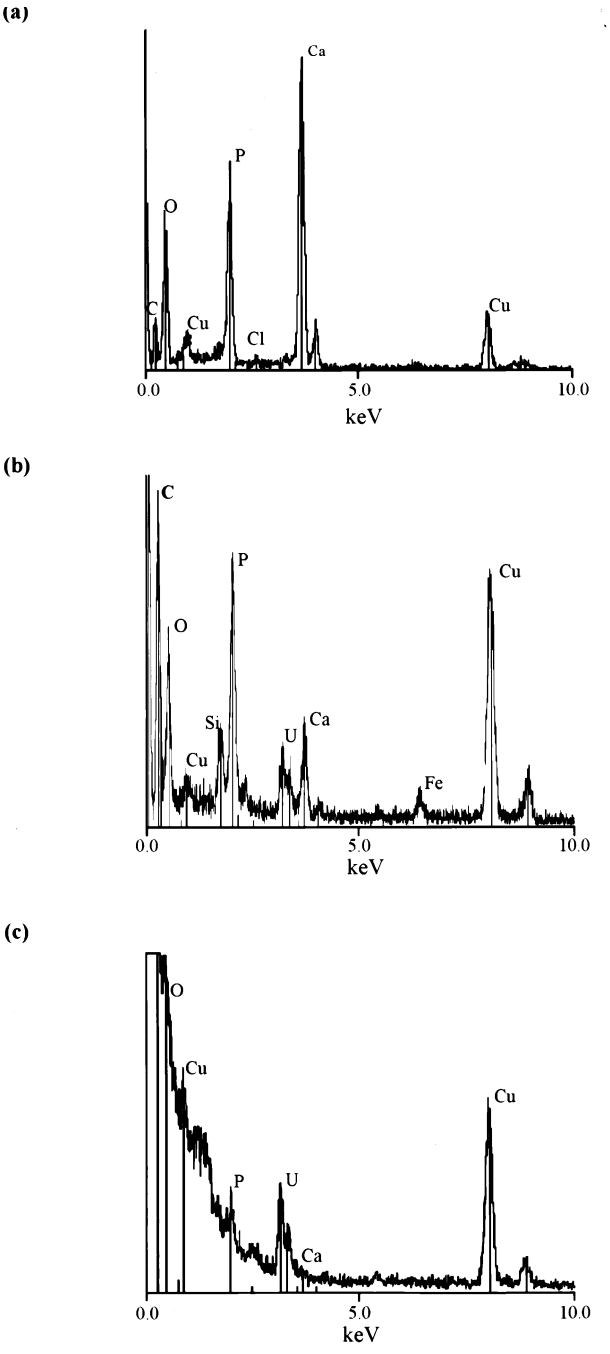

Fig. 4. EDS spectrum showing the chemical composition of nanoform type 1: (a) before removal of mineral, (b) after immunolabeling, and (c) after mineral dissolution. The presence and relative quantities of P, Ca, and O peaks in (a) indicate that nanoform type 1 has a mineral composition typical of carbonated hydroxyapatite. The C peak is due partially to the presence of an organic phase, whereas the Cu peak derives from the Cu grid. Preparation for the immuno-gold labeling resulted in partial dissolution of the mineral phase, especially the depletion of Ca (c). The C content visible in the spectra indicates an intimate association of an organic phase with the mineral (b and c). Uranium in (b) and (c) is from uranyl acetate staining, whereas the Si and Fe in (b) are due to contamination during immunolabeling.

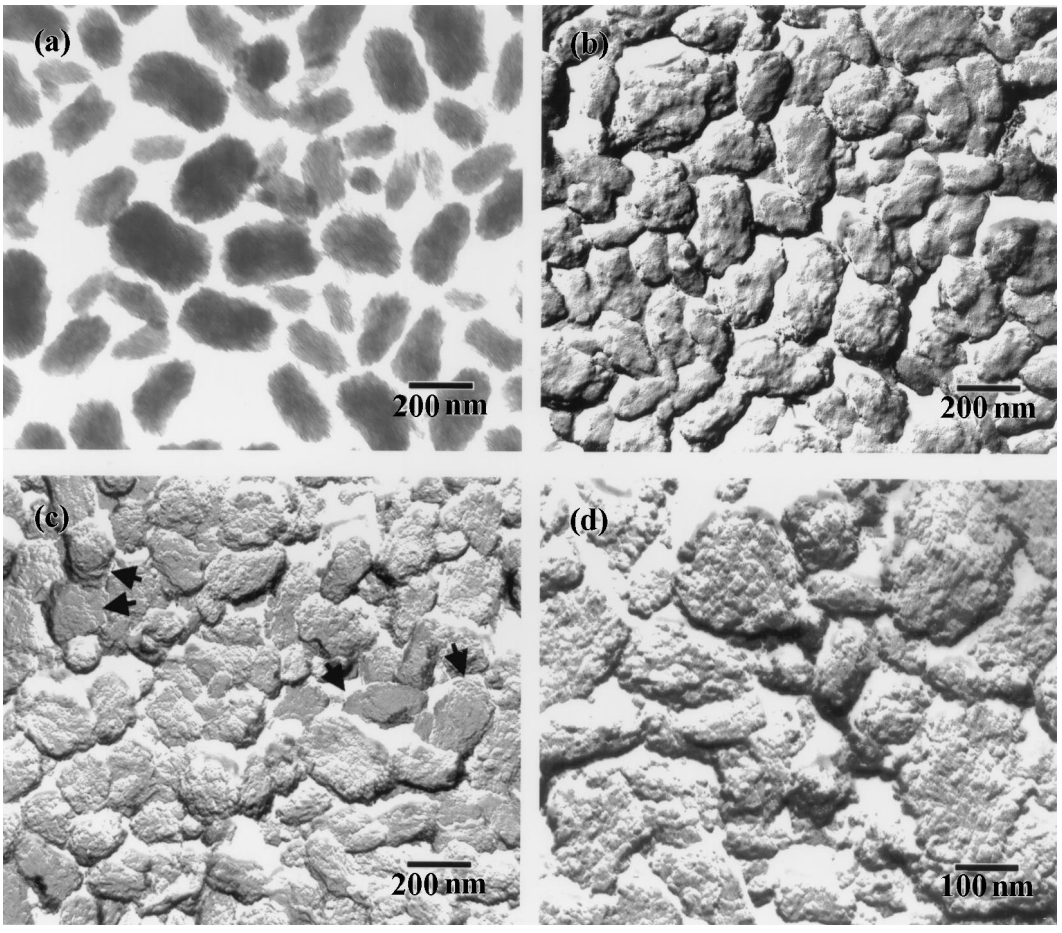

Fig. 5. TEM images of nanoform type 1 obtained from the 1:10 FBS/DMEM mixture cultures: (a) Air-dried nanoform type 1 adsorbed onto a formvar–carbon supported grid. (b) Pt–C replica obtained from freeze-etched pellet of the same culture as (a) shows the surface topography of nanoform type 1. (c) Freeze-fractured pellet shows the layered surface (arrows) and internal structure of individual nanoforms. (d) High-resolution TEM image of the fractured surface reveals the crystalline nature of nanoform type 1. Cellular structures are not visible in this specimen.

An additional, nonmineralized spherical nanoform, here referred to as nanoform type 2, was sometimes observed in normal samples by using TEM (Fig. 8a). This form was present in both pure FBS and in 1:10 FBS/DMEM mixtures. Immunogold labeling of a specimen containing nanoform types 1 and 2 showed a response for nanoform type 1 only (Fig. 8b). Using high-speed centrifugation, samples were enriched in nanoform type 2. Although it was not possible to prepare ultrathin sections of these forms to study their internal structure, ultrathin sections of monolayers that adhered to the bottom of the container of a 4-week-old culture revealed well-preserved, membrane-like structures (Fig. 9a,b). The size distribution of these forms was similar to that observed for nanoform type 2. The mineralization pattern of the adhering species appears to be distinct from that of the dispersed and free nanoforms in the culture solution. It is possible that an association exists between nonmineralized and mineralized nanoforms. More detailed studies are required, however, to establish this relationship.

When the concentration of FBS was less than 10% of the growth medium, most of the material adhered to the incubation vessel. The concentration of FBS was extensively reduced by replacing the 1:10 FBS/DMEM mixture with pure DMEM. After repeating this procedure 10 times, the adhered material is described as serum-free (SF) culture (Kajander and Çiftçioglu, 1998). In the SF environment, semispherical forms up to 10 μm in diameter were formed (Fig. 10a). Figure 10b is a TEM image of a cross-section of an SF form showing the internal structure. The size and shape of HAP crystals were similar to the small, adhered nanoforms observed in the FBS/DMEM medium (Fig. 9a,b). At least two types of crystal forms were observed in both nanoforms and SF forms; plate-like HAP crystals and a fine-grained calcium phosphate that appears to be more concentrated toward the center of the forms. HRTEM revealed, however, that both types of crystals were present throughout the nanoforms and SF forms.

4. DISCUSSION

The precipitation of HAP in serum leading to the formation of nanoforms has been attributed to nan(n)obacteria (Kajander and Çiftçioglu, 1998). Owing to the size and paucity of biochemical data and the lack of cellular structures, however, the origin of these nanoforms remains controversial. Nevertheless, understanding the processes of formation of HAP in serum has

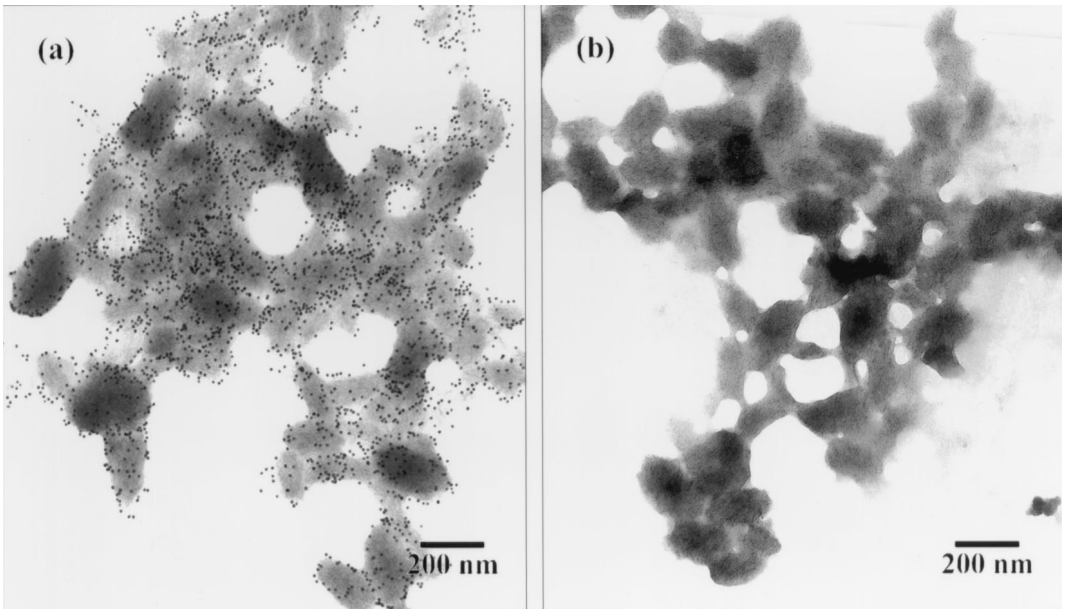

Fig. 6. TEM image of nanoform type 1 adsorbed onto a formvar-supported grid. (a) Immuno-gold labeled proteinaceous remnant of nanoform type 1 exposed to monoclonal antibody Nb 8/0 (10 nm-sized gold particles). (b) Control specimen without exposure to the primary antibody.

implications for evaluating the nanoscale features described in geological samples as mineralized nan(n)obacteria (Folk, 1993; McKay et al., 1996; Uwins et al., 1998). Mineralization in bacteria can occur within the cell or on the cell walls (e.g., Blakemore, 1975; Lowenstam, 1986; Lowenstam and Weiner, 1989; Vali and Kirschvink, 1990; Warren and Ferris, 1998). In either event, one would expect to be able to observe examples of the progressive mineralization of cellular structure from

Table 2. Biochemical profile of fetal bovine serum (FBS) before and after incubation.

		Experiment 1		Experiment 2	
Test description[a]	Units	Control[b]	Incubated[c]	Control[b]	Incubated[c]
CO_2 content	mmol/L	21	17	21	18
Sodium	mmol/L	146	150	149	153
Potassium	mmol/L	6.3	6.6	6.5	6.7
Chloride	mmol/L	114	116	117	119
Uric acid	mg/dL	<0.3	<0.3	<0.3	0.3
Phosphorus	mg/dL	8.8	7.2	8.8	6.4
Calcium	mg/dL	10.0	5.6	11.4	5.1
Alkaline phosphatase	u/L	234	49	244	43
GGT	u/L	397	356	510	394
AST (SGOT)	u/L	6	3	5	3
ALT (SGPT)	u/L	9	2	10	4
LDH	u/L	327	218	334	212
Total bilirubin	mg/dL	0.4	0.5	0.3	0.3
Glucose	mg/dL	106	108	127	122
BUN	mg/dL	13	14	12	13
Creatinine	mg/dL	0.9	1.5	0.9	1.5
Cholesterol	mg/dL	66	68	68	66
HDL cholesterol	mg/dL	48	50	51	48
Triglycerides	mg/dL	41	53	51	55
Iron	mcg/dL	97	118	99	104
TIBC	mcg/dL	472	461	486	435
Transferrin saturation	%	21	26	20	24

[a] GGT: gamma glutamyl transpeptidase; AST (SGPT), serum glutamate pyruvate transferase; ALT (SGOT), serum glutamate oxalate transferase; LDH, lactate dehydrogenase; BUN, blood urea nitrogen; HDL, high density lipoprotein; TIBC, total iron binding capacity

[b] Control: Original FBS

[c] Incubated: same as control after 3 weeks of incubation/growth. The precipitate was removed by centrifugation and supernatant collected for analysis by LPGC.

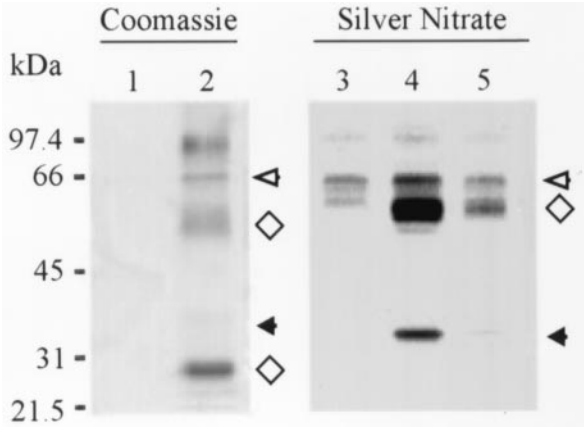

Fig. 7. Immunoprecipitation of purified protein sample from mineralized material purified by the procedure described in Analytical Techniques. Lane 1: Protein G Sepharose beads were incubated with the sample. Lane 2: immunoprecipitate of the purified sample by the antibody Nb 8/0. After resolution by SDS-polyacrylamide gel electrophoresis, proteins were visualized by Coomassie Blue R250 staining. Lane 3: lane 1, but with silver nitrate staining. Lanes 4 and 5: immunoprecipitate of the purified material by the antibody Nb 5/2 in native and denaturing conditions, respectively. The light and heavy Ig chains are shown by diamonds. Open arrows indicate the nonspecific bands, and solid arrows indicate proteins of interest.

nan(n)obacteria to mineralized nanoform, as has been shown in in vitro precipitation of HAP by *Escherichia coli* and *Streptococcus* bacteria (Ennever et al., 1974; Streckfuss et al., 1974). The direct mineralization of nan(n)obacteria leading to the formation of nanoforms, therefore, can be excluded. On the other hand, the nonmineralized forms (nanoform type 2) with a membrane-bound structure seen in Figures 8 and 9 resemble some bacteria. The size of these forms (30–150 nm), however, is smaller than any known microorganism. The origins of these forms and their role in the mineralization, as well as 16S rRNA gene sequencing, DNA staining, and metabolic labeling reported by Kajander & Çiftçioglu (1998), cannot be explained at this time. Therefore, conventional biomineralogical and biogeochemical techniques, as well as recently developed thermodynamic and kinetic models (Fein et al., 1997; Warren and Ferris, 1998; Fein and Delea, 1999) that have been employed to study bacteria induced or controlled mineralization, cannot be applied to the system described here.

Geochemical analysis is conventionally used to investigate processes of mineralization in aqueous solution. Ideally, the kinetics of reaction are studied in a simple system where there are a limited number of parameters that can be easily controlled. However, studying the kinetics of reaction leading to co-precipitation of HAP and protein phases (nanoforms) in serum based on solution chemistry by using a geochemical approach is extremely difficult. Therefore, the focus of this article was to describe the structure and composition of the solid phase (nanoforms) by using structural and biochemical techniques. The FBS/DMEM mixture containing [Ca] 2.1 mM was probably not supersaturated with respect to the nucleation of HAP and the growth of nanoforms. The control experiment using DMEM did not result in the nucleation of nanoforms. If DMEM was seeded with nanoforms, however, formation of HAP crystals was observed. Inorganic precipitation of HAP with similar morphology has been reported in solutions containing [Ca] 8.0 mM and [P] 3.4 mM (Eanes et al., 1973). In contrast to our system, a phase transformation from amorphous calcium phosphate to crystalline HAP occurs at neutral pH in the inorganic synthesis of HAP. Although [Ca] 1.8–2.1 mM and [P] 0.8–0.9 mM in our system may be saturated with respect to HAP (Eidelman et al., 1987), nucleation and growth of HAP in growth medium with similar [Ca] and [P] did not occur. It is important to note that the exposure of inorganic HAP crystals into FBS and DMEM resulted in their partial dissolution indicating that both solutions are undersaturated with respect to HAP. It is evident, therefore, that the nucleation of HAP in nanoforms requires the involvement of organic macromolecules such as proteins and other biogenic molecules present in serum and in growth medium.

The ability of proteins to control the nucleation, growth, alignment, and morphology of crystals during biomineralization represents an important evolutionary trait among various

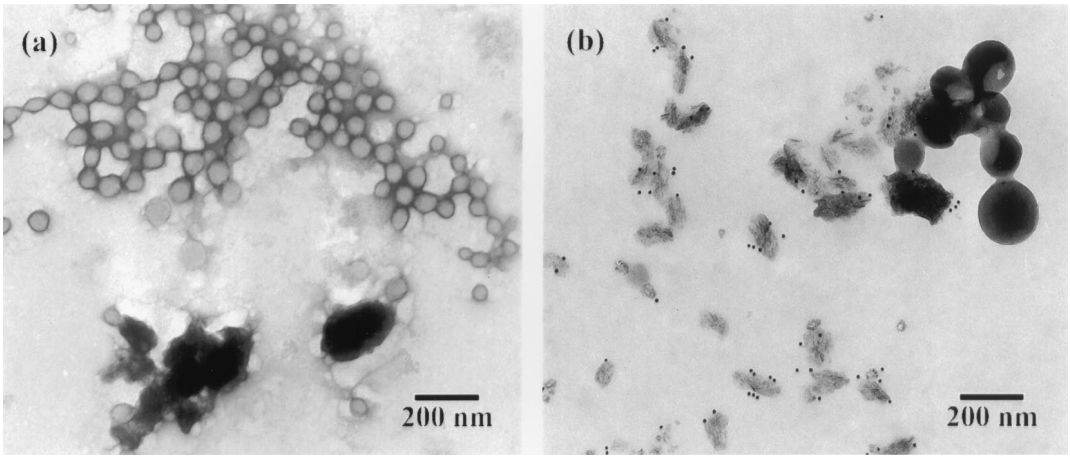

Fig. 8. TEM images of a specimen containing nanoform types 1 and 2: (a) Negatively stained nanoform type 2 adsorbed on carbon film. (b) Immuno-gold labeled specimen using monoclonal antibody Nb 8/0 shows the association of the monoclonal antibody with nanoform type 1 only.

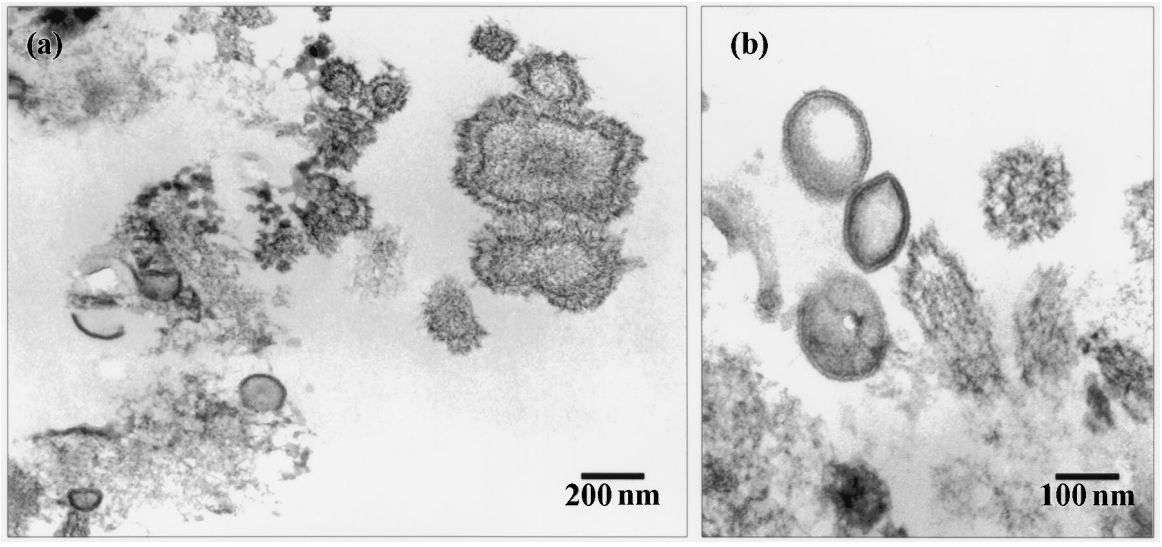

Fig. 9. TEM images of ultrathin sections of monolayers that adhere to the bottom of the container of a 4-week-old SF culture (nanoforms were isolated from the 1:10 FBS/DMEM mixture and added to serum-free DMEM growth medium). (a) Cross-section of a monolayer shows the internal structure of mineralized and nonmineralized forms. (b) Higher magnification of the same specimen shows the well-preserved membrane structure of a "vesicle" and different degrees of mineralization of the nanoforms. It appears that the mineralization process in SF cultures is distinct from the serum containing cultures described above.

diverse organisms across numerous phyla (Berman et al., 1990; Mann et al., 1991; Hunter et al., 1996; Walters et al., 1997; Mann and Weiner, 1999). Conversely, crystal surfaces are known to affect protein conformation after their adsorption (Ferris et al., 1996; Ertem and Ferris, 1998; Long et al., 1998). The crossover of organic and inorganic reactions is of great interest, not only for certain growing biotechnology industries and large-scale commercial bioprocesses, but also for something as primal as the very origins of life itself. One of the hypotheses for the origin of life involves the ordering and possible catalytic polymerization of amino acids and/or oligopeptides at an inorganic interface (Cairns-Smith, 1982; Huber and Wächterhäuser, 1997; Orgel, 1998a; Ferris, 1999). Imai et al. (1999) modeled a method that could explain the formation of stable oligopeptides in the presence of copper ions given an energy source such as a submarine hydrothermal vent system.

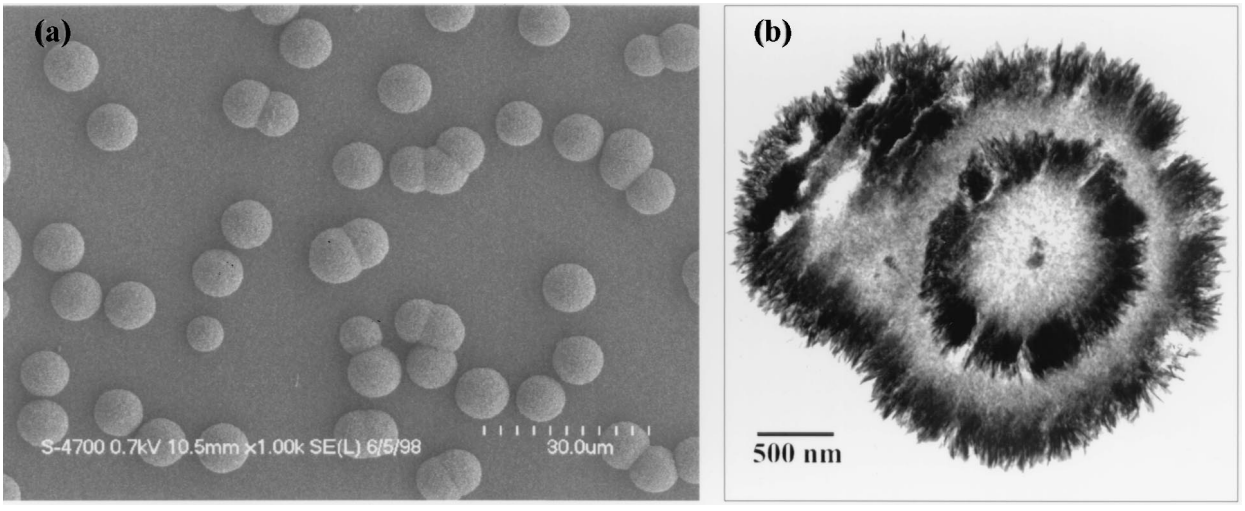

Fig. 10. (a) field emission gun SEM image of semispherical forms formed in SF medium. The roughness of the surface represents the arrangement of HAP crystals that may have been altered by dehydration in vacuum. (b) TEM image of an ultrathin section obtained from a similar monolayer as in (a), showing the internal structure of these forms. The plate-like HAP crystals on the outer edge of the form are similar to nanoform type 1. The inner ring shows the earliest stage of growth followed by overgrowth in the later stage. The accumulation of fine-grained crystals in the center and middle of the form may represent a secondary phase subsequently altered from its original state. Partial dissolution of both types of crystals during ultrathin sectioning cannot be excluded.

Apatite crystals are routinely used for the polymerization of amino acids (Hill et al., 1998; Orgel, 1998b). It is likely that in the prebiotic world, apatite served as a substrate for the formation of oligonucleotides or oligopeptides. Once formed, organic moieties can survive geological events and provide useful biogenetic information. Preservation of ancient macromolecules, such as nucleic acids, proteins, and polysaccharides, has been demonstrated (Robbins and Brew, 1990; Logan et al., 1991). Indeed, proteins recovered from dinosaur bones are immunologically reactive to antibodies raised against mineral-binding bone proteins of modern vertebrates, an observation useful not only for elucidating molecular phylogeny, but for demonstrating the protective nature of mineral interfaces (Muyzer et al., 1992). For the nanoforms in the present study, it would be entirely possible that the protein-mineral interactions might be similar. Likewise, it is possible that the HAP present in the nanoforms acts to stabilize the organic phase under harsh environmental conditions. Interestingly, intracellular biocrystallization of the nonspecific DNA-binding protein Dps has been shown to provide protection of DNA against oxidative agents under extreme conditions (Grant et al., 1998; Wolf et al., 1999). In the absence of well-preserved microfossils, biomarkers are used to recognize biological activities in geological systems. The association of proteins or peptides and other macromolecules with HAP crystals leading to the formation of nanoforms has implications for studying biomarkers in ancient terrestrial and extraterrestrial environments.

The increase in the number of HAP crystals is responsible for the growth of nanoforms rather than the increase in size of individual crystals. This implies continuous nucleation concomitant with inhibition. The mineralization process, therefore, is most likely regulated by the resident organic phase. Protein-based mechanisms underlying the mineralization of nanoforms may be common to similar fundamental processes occurring in vertebrate calcified tissues such as bones and teeth (Aoba et al., 1991; Boskey et al., 1993; Taira et al., 1995; Hunter, 1996; Hunter et al., 1996; Moradian-Oldak et al., 1998a,b). In these tissues, similar nanometer-scale HAP crystals form aggregates that, likewise, are intimately associated with organic molecules at crystal surfaces (Bonucci et al., 1988; McKee and Nanci, 1995). As for the nanoforms described here, repeated nucleation and inhibition of crystal growth occurs simultaneously. Thus new crystals are continually formed de novo, but then inhibited from further growth after reaching a critical size. This process, in turn, requires the continuous availability of mineral-binding, regulatory molecules (e.g., phospholipids, proteins, peptides, and amino acids). Similar fundamental mechanisms may be operative in nanoforms because crystal growth not regulated in a biogenic manner would lead to fewer and much larger crystals.

For matrix-mediated guidance of mineralization in vertebrates, recent studies in vitro (Hunter and Goldberg, 1994; Hunter et al., 1994) have identified the importance of carboxylate and phosphate groups on specific proteins. Requirements for secondary structure related to those functional groups for these and other proteins have not been determined. Other proposals for the regulation of HAP mineralization have arisen from the detection of small vesicles in cartilage that detach from chondrocytes, mineralize, and are otherwise known as matrix vesicles (Sela et al., 1992; Wuthier et al., 1992; Anderson, 1995). Moreover, significant work has been performed on microbial apatitic calcification (Vogel and Boyan-Salyers, 1976). In the latter two cases, it has been proposed that acidic phospholipids in membranes associate with specific proteolipids to form a complex that directs the initial phases of mineralization in these biological systems (van Dijk et al., 1998). Thus, the fundamental interactions between protein and crystal surfaces, in light of nucleating potential and inhibitory activity, may be similar between nanoforms and matrix-mediated calcification in vertebrates, rather than being induced by vesicles or bacteria. We note, however, that the nature of the nanoforms as isolated entities not intimately embedded within a classical, fibrillar extracellular matrix with associated cells is unique compared to other known matrix-controlled mineralization systems. In terms of the mineralization process leading to the formation of nanoforms, the possibility that crystallites arising from generally serum-depleted incubation conditions, yet exposed to the organic elements of various growth media, may allow self-assembly of amino acids onto crystal surfaces cannot be excluded (Kresak et al., 1977). This process may mimic in a more primitive manner the functionality achieved by proteins in more complex biological systems. The ordered structure observed in freeze-fractured replicas suggests the occurrence of a self-assembly mode of formation of the nanoform through a simultaneous accumulation of mineral and protein. The fact that nanoform type 1 is present as free particles suggests that it forms as colloidal entities in solution. It is likely that individual macromolecules or aggregates of smaller organic molecules serve as nucleation sites for the formation of HAP. As crystals of HAP grow, both inorganic ions and organic molecules in the serum may interact with the surfaces of the crystal and further growth may be inhibited in some crystallographic directions. This has been well documented in studies of larger crystals and may explain the preferential growth or inhibition of distinct crystals faces (e.g., Mann et al., 1993; Paquette et al., 1996). Indeed, it has been well documented that minor amounts of Mg or Na, which are present in nanoform type 1, strongly affect crystal growth (e.g., Paquette et al., 1996). This mechanism, however, fails to fully explain the continuous nucleation and inhibition that results in the restriction of crystal size in nanoform type 1.

5. CONCLUSIONS

The results presented here show a previously unknown type of protein–mineral formation described as nanoforms. Distinct nano-phenomena have been widely interpreted as being living organisms. As we were unable to observe any cellular structure associated with mineralization leading to the formation of nanoforms, it must be concluded that nan(n)obacteria were not present in our system. Although we occasionally observed membrane-like features (nanoform type 2), without knowing their composition and detailed structure, we cannot describe them as being derived from living entities. Although there is evidence for the association of protein with the formation of HAP in nanoform type 1 in serum-containing media, the growth of HAP with similar composition in SF medium suggests that in the process of calcification other macromolecules may serve as nucleation sites. Without biochemical data, therefore, caution must be exercised in ascribing similar features as

biomarkers in geological systems. If the association of protein phases with mineralization processes leading to the formation of similar nanoforms can be established, it may be an alternative mechanism of formation for the nanoscale features reported in various geological samples. In addition, the formation of HAP in serum culture offers a unique opportunity to study under laboratory conditions the calcification processes in tissues. This study demonstrated that combined biochemical, geochemical, and mineralogical analyses are required for the investigation of processes of mineralization in both biological and geological complex systems.

Acknowledgments —We are grateful to Hitachi Sangyo Canada, Inc., for arranging the use of the field emission gun SEM. We also thank Prof. John J. M. Bergeron and three anonymous reviewers for their critical comments. The research was made possible by financial support from NSERC to Hojatollah Vali.

REFERENCES

Anderson H. C. (1995) Molecular biology of matrix vesicles. *Clin. Orthop.* **314,** 266–280.

Aoba T., Miake Y., Shimoda S., Prostak K., Moreno E. C., and Suga S. (1991) Dental apatites in vertebrate species: Morphology and chemical properties. In *Mechanisms and Phylogeny of Mineralization in Biological Systems* (ed. S. Suga and H. Nakahara), pp. 459–463. Springer–Verlag, Tokyo.

Bachmann L. (1987) Freeze-etching of dispersions, emulsions and macromolecular solutions of biological interest. In *Cryotechniques in Biological Electron Microscopy* (ed. R. A. Steinbrecht and K. Zierold). pp. 192–204. Springer–Verlag, New York,

Berman A., Addadi L., Kvick Å., Leiserrowitz L., Nelson M., and Weiner S. (1990) Intercalation of sea urchin proteins in calcite: Study of a crystalline composite material. *Science* **250,** 664–667.

Blakemore R. P. (1975) Magnetotactic bacteria. *Science* **190,** 377–379.

Bonucci E., Silvestrini G., and Di Grezia R. (1988) The ultrastructure of the organic phase associated with the inorganic substance in calcified tissues. *Clin. Orthop.* **233,** 243–261.

Boskey A. L. Maresca M., Ullrich W., Doty S. B., Butler W. T., and Prince C. W. (1993) Osteopontin-hydroxyapatite interactions in vitro: Inhibition of hydroxyapatite formation and growth in a gelatin-gel. *Bone Miner.* **22,** 147–159.

Bradley J. P., Harvey R. P., and McSween H. Y. Jr. (1997) No 'nanofossils' in martian meteorite. *Nature* **390,** 454.

Cairns-Smith A. G. (1982) *Genetic Takeover and the Mineral Origins of Life.* Cambridge University Press.

Çiftçioglu N., Bjorklund M., Kuoriksoski K., Bergstrom K., and Kajander E. O. (1999) Nanobacteria: An infectious cause for kidney stone formation. *Kidney Int.* **56,** 1893–1898.

de Duve C. and Osborn M. J. (1999) Panel 1: Discussion. In *Size Limits of Very Small Microorganisms: Proceedings of a Workshop.* Steering Group for the Workshop on Size Limits of Very Small Microorganisms, National Research Council, Space Studies Board. National Academy Press, Washington, D.C.

Eanes E. D., Termine J. D., and Nylen M. U. (1973) An electron microscopic study of the formation of amorphous calcium phosphate and its transformation to crystalline apatite. *Calc. Tiss. Res.* **12,** 143–158.

Eidelman N., Chow L. C., and Brown W. E. (1987) Calcium phosphate saturation levels in ultrafiltered serum. *Calc. Tiss. Int.* **40,** 71–78.

Ennever J., Vogel J. J., and Streckfuss J. L. (1974) Calcification by *Escherichia coli. J. Bacter.* **119,** 1061–1062.

Ertem G. and Ferris J. P. (1998) Formation of RNA oligomers on montmorillonite: Site of catalysis. *Orig. Life Evol. Biosph.* **28,** 485–499.

Fein J. B., Daughney C. J., Yee N., and Davis T. (1997) A chemical equilibrium model of metal adsorption onto bacterial surfaces. *Geochim. Cosmochim. Acta* **162,** 33–45.

Fein J. B. and Delea D. (1999) Experimental study of the effect of EDTA on Cd adsorption by Bacillus subtilis: A test of the chemical equilibrium approach. *Chem. Geol.* **161,** 375–383.

Ferris J. P. (1999) Prebiotic synthesis on minerals: Bridging the prebiotic and RNA worlds. *Biol. Bull.* **196,** 311–314.

Ferris J. P., Hill A. R. Jr., Liu R., and Orgel L. E. (1996) Synthesis of long prebiotic oligomers on mineral surfaces. *Nature* **381,** 59–61.

Folk R. L. (1993) SEM imaging of bacteria and nannobacteria in carbonate sediments and rocks. *J. Sed. Petrol.* **63,** 990–999.

Folk R. L. (1997) Nannobacteria: Size limits and evidence. *Science* **276,** 1776–1777 (Letter).

Folk R. L. and Lynch F. L. (1997) The possible role of nannobacteria (dwarf bacteria) in clay-mineral diagenesis and the importance of careful sample preparation in high magnification SEM study. *J. Sed. Res.* **67,** 583–589.

Grant R. A., Filman D. J., Finkel S. E., Kolter R., and Hogle J. M. (1998) The crystal structure of Dps, a ferritin homolog that binds and protects DNA. *Nat. Struct. Biol.* **5,** 294–303.

Hill A. R., Jr., Böhler C., and Orgel L. E. (1998) Polymerization on the rocks: Negatively-charged α-amino acids. *Origins Life Evol. Biosph.* **28,** 235–243.

Hjelle J. H., Miller-Hjelle M. A., Poxton I. R., Kajander E. O., Çiftçioglu N., Jones M. J., Caughey R. C., Brown R., Millikin P. D., and Darras F. S. (2000) Endotoxin and nanobacteria in polycystic kidney disease. *Kidney Inter.* **57,** 2360–2374.

Huber C. and Wächterhäuser G. (1997) Activated acetic acid by carbon fixation on (Fe,Ni)S under primordial conditions. *Science* **276,** 245–247.

Hunter G. K. (1996) Interfacial aspects of biomineralization. *Curr. Opin. Solid State Mater. Sci.* **1,** 430–435.

Hunter G. K. and Goldberg H. A. (1994) Modulation of crystal formation by bone phosphoproteins: Role of glutamic acid-rich sequences in the nucleation of hydroxyapatite by bone sialoprotein. *Biochem. J.* **302,** 175–179.

Hunter G. K., Hauschka P. V., Poole A. R., Rosenberg L. C., and Goldberg H. A. (1996) Nucleation and inhibition of hydroxyapatite formation by mineralized tissue proteins. *Biochem. J.* **317,** 59–64.

Hunter G. K., Kyle C. L., and Goldberg H. A. (1994) Modulation of crystal formation by bone phosphoproteins: Structural specificity of the osteopontin-mediated inhibition of hydroxyapatite formation. *Biochem. J.* **300,** 723–728.

Imai E., Honda H., Hatori K., Brack A., and Matsuno K. (1999) Elongation of oligopeptides in a simulated submarine hydrothermal system. *Science* **283,** 831–833.

Kajander E. O. and Çiftçioglu N. (1998) Nanobacteria: An alternative mechanism for pathogenic intra- and extracellular calcification and stone formation. *Proc. Natl. Acad. Sci. USA* **95,** 8274–8279.

Kresak M., Moreno E. C., Zahradnik R. T., and Hay D. I. (1977) Adsorption of amino acids onto hydroxyapatite. *J. Colloid. Interface Sciences* **59,** 283–292.

Laemmli U. K. (1970) Cleavage of structural proteins during the assembly of the head of bacteriophage T4. *Nature* **227,** 680–685.

Logan G. A., Collins M. J., and Eglinton G. (1991) Preservation of organic biomolecules. In *Taphonomy: Releasing the Data Locked in the Fossil Record* (eds. P. Allison and D. Briggs). pp. 1–24. Plenum Press.

Long J. R., Dindot J. L., Zebroski H., Kine S., Clark R. H., Campbell A. A., Stayton P. S., and Drobny G. P. (1998) A peptide that inhibits hydroxyapatite growth is in an extended conformation on the crystal surface. *Proc. Natl. Acad. Sci. USA* **95,** 12083–12087.

Lowenstam H. A. (1981) Minerals formed by organisms. *Science* **211,** 1126–1131.

Lowenstam H. A. (1986) Mineralization processes in monerans and protoctists. In *Biomineralization in Lower Plants and Animals. Proceedings of an International Symposium Held at the University of Birmingham, 15–19 April 1985.* (eds. B. S. C. Leadbeater and R. Riding). pp. 1–17. Published for the Systematics Association by the Clarendon Press, New York: Oxford University Press.

Lowenstam H. A. and Weiner S. (1989) *On Biomineralization.* Oxford University Press.

Maniloff J. (1997) Nannobacteria: Size limits and evidence. *Science* **276,** 1776–1777 (Letter).

Mann S., Archibald D. D., Didymus J. M., Douglas T., Heywood B. R., Meldrum F. C., and Reeves N. J. (1993) Crystallization at inorganic-

organic interfaces: Biominerals and biomimetic synthesis. *Science* **261,** 1286–1292.

Mann S., Heywood B. R., Rajam S., and Wade V. J. (1991) Molecular recognition in biomineralization. In *Mechanisms and Phylogeny of Mineralization in Biological Systems* (ed. S. Suga and H. Nakahara). pp. 47–56. Springer–Verlag, Tokyo.

Mann S. and Ozin G. A. (1996) Synthesis of inorganic materials with complex form. *Nature* **382,** 313–318.

Mann S. and Weiner S. (1999) Biomineralization: Structural questions at all length scales. *J. Struct. Biol.* **126,** 179–181.

McKay D. S., Gibson E. K. Jr., Thomas-Keprta K. L., Vali H., Romanek C. S., Clemett S. J., Chillier X. D. F., Maechling C. R., and Zare R. N. (1996) Search for past life on Mars: Possible relic biogenic activity in martian meteorite ALH84001. *Science* **273,** 924–930.

McKee M. D. and Nanci A. (1995) Postembedding colloidal-gold immunocytochemistry of noncollagenous extracellular matrix proteins in mineralized tissues. *Microsc. Res. Tech.* **31,** 44–62.

Moor H. and Muehlethaler K. (1963) Fine structure in frozen-etched yeast cells. *J. Cell Biol.* **17,** 609–628.

Moradian-Oldak J., Leung W., and Fincham A. G. (1998a) Temperature and pH-dependent supramolecular self-assembly of amelogenin molecules: A dynamic light-scattering analysis. *J. Struct. Biol.* **122,** 320–327.

Moradian-Oldak J., Tan J., and Fincham A. G. (1998b) Interaction of amelogenin with hydroxyapatite crystals: An adherence effect through amelogenin molecular self-association. *Biopolymers* **46,** 225–238.

Muyzer G., Sandberg P., Knapen M. H., Vermeer C., Collins M., and Westbroek P. (1992) Preservation of the bone protein osteocalcin in dinosaurs. *Geology* **20,** 871–874.

Nealson K. (1997) Nannobacteria: Size limits and evidence. *Science* **276,** 1776–1777 (Letter).

Nealson K. (1999) Panel 2: Discussion. In *Size Limits of Very Small Microorganisms: Proceedings of a Workshop.* Steering Group for the Workshop on Size Limits of Very Small Microorganisms, National Research Council, Space Studies Board. National Academy Press, Washington, D.C.

Oliver S., Kuperman A., Coombs N., Lough A., and Ozin G. A. (1995) Lamellar aluminophosphates with surface patterns that mimic diatom and radiolarian microskeletons. *Nature* **378,** 47–50.

Orgel L. E. (1998a) The origin of life—A review of facts and speculations. *TIBS.* **23,** 491–495.

Orgel L. E. (1998b) Polymerization on the rock: Theoretical introduction. *Orig. Life Evol. Biosph.* **28,** 227–234.

Orgel L. E. and Ost L. (1999) Panel 4: Discussion. In *Size Limits of Very Small Microorganisms: Proceedings of a Workshop.* Steering Group for the Workshop on Size Limits of Very Small Microorganisms, National Research Council, Space Studies Board. National Academy Press, Washington, D.C.

Pace N. R. (1997) Secular view of microbial diversity and the biosphere. *Science* **276,** 734–740.

Paquette J., Vali H., and Mountjoy E. W. (1999) Novel TEM approaches to imaging of microstructures in carbonates: Growth mechanisms in calcite and dolomite. *Am. Mineral.* **84,** 1939–1949.

Paquette J., Vali H., and Mucci A. (1996) TEM study of Pt-C replicas of calcite overgrowths precipitated from electrolyte solutions. *Geochim. Cosmochim. Acta* **60,** 4689–4699.

Pedone V. A. and Folk R. L. (1996) Formation of aragonite cement by nannobacteria in the Great Salt Lake, Utah. *Geology* **24,** 763–765.

Psenner R. and Loferer M. (1997) Nannobacteria: Size limits and evidence. *Science* **276,** 1776–1777 (Letter).

Robbins L. L. and Brew K. (1990) Proteins from the organic matrix of core-top and fossil planktonic foraminifera. *Geochim. Cosmochim. Acta* **54,** 2285–2229.

Sela J., Schwartz Z., Swain L. D., and Boyan B. D. (1992) Role of matrix vesicles in calcification. In *Calcification in Biological Systems* (ed. E. Bonucci). pp. 73–105. CRC Press.

Sillitoe R. H., Folk R. L., and Saric N. (1996) Bacteria as mediators of copper sulfide enrichment during weathering. *Science* **272,** 1153–1155.

Streckfuss J. L., Smith W. N., Brown L. R., and Campbell M. M. (1974) Calcification of selected strains of *Streptococcus mutans* and *Steptococcus sanguis. J. Bacter.* **120,** 502–506.

Taira T., Iijima M., Moriwaki Y., and Kuboki Y. (1995) A new method for in vitro calcification using acrylamide gel and bovine serum. *Connect. Tissue Res.* **33,** 185–192.

Uwins P. J. R., Webb R. I., and Taylor A. P. (1998) Novel nano-organisms from Australian sandstones. *Am. Mineral.* **83,** 1541–1550.

Vali H. and Bachmann L. (1988) Ultrastructure and flow behaviour of colloidal smectite dispersions. *J. Colloid. Interface Sci.* **126,** 278–291.

Vali H., Hesse R., and Kohler E. E. (1991) Combined freeze-etch replicas and HRTEM images as tools to study fundamental particles and the multiphase nature of 2:1 layer silicates. *Am. Mineral.* **76,** 1973–1984.

Vali H. and Kirschvink J. (1990) Observations of magnetosome organization, surface structure, and iron biomineralization of undescribed magnetic bacteria: Evolutionary speculations. In *Iron Biominerals* (eds. R. B. Frankel and R. P. Blakemore). pp. 97–115. Plenum Press.

Vali H., Sears S. K., Çiftçioglu N., and Kajander E. O. (1999) *Nanofossils and the size limits of life.* pp. 1890–1891. 30th Lunar and Planetary Science Conference, Houston.

van Dijk S., Dean D. D., Liu Y., Zhao Y., Chirgwin J. M., Schwartz Z., and Boyan, B. D. (1998) Purification, amino acid sequence, and cDNA sequence of a novel calcium-precipitating proteolipid involved in calcification of *Corynebacterium matruchotii. Calcif. Tissue Int.* **62,** 350–358.

Vogel J. J. and Boyan-Salyers B. D. (1976) Acidic lipids associated with the local mechanism of calcification: A review. *Clin. Orthop.* **118,** 231–241.

Walters D. A., Smith B. L., Belcher A. M., Paloczi G. T., Stucky G. D., Morse D. E., and Hansma P. K. (1997) Modification of calcite crystal growth by abalone shell proteins: An atomic force microscope study. *Biophys. J.* **72,** 1425–1433.

Warren L. A. and Ferris F. G. (1998) Continuum between sorption and precipitation of Fe(III) on microbial surfaces. *Environ. Sci. Technol.* **32,** 2331–2337.

Wolf S. G., Frenkiel D., Arad T., Finkel S. E., Kolter R., and Minsky A. (1999) DNA protection by stress-induced biocrystallization. *Nature* **400,** 83–85.

Wuthier R. E., Wu L. N., Sauer G. R., Genge B. R., Yoshimori T., and Ishikawa Y. (1992) Mechanism of matrix vesicle calcification: Characterization of ion channels and the nucleational core of growth plate vesicles. *Bone Miner.* **17,** 290–295.